Environmental Science and Pollution Research (2018) 25:26114–26134
https://doi.org/10.1007/s11356-018-2566-1

RESEARCH ARTICLE

Application of Box–Behnken design and desirability function in the optimization of Cd(II) removal from aqueous solution using poly(o-phenylenediamine)/hydrous zirconium oxide composite: equilibrium modeling, kinetic and thermodynamic studies

Nafisur Rahman[1] · Mohd Nasir[1]

Received: 25 April 2018 / Accepted: 13 June 2018 / Published online: 3 July 2018

Abstract

In this research work, poly(o-phenylenediamine) was incorporated into the hydrous zirconium oxide matrix to form poly(o-phenylenediamine)/hydrous zirconium oxide composite which is used for the removal of Cd(II) from aqueous solution. The characterization of the material was done based on FTIR, XRD, SEM, and TGA-DTA. The effects of contact time, pH, adsorbent dose, and initial concentration of Cd(II) on the removal of Cd(II) were studied by performing 29 sets of sorption runs using Box–Behnken design combined with response surface methodology (RSM). Various isotherm models were tested to describe the adsorption equilibrium. The adsorption equilibrium data fitted well with Freundlich isotherm model. The maximum adsorption capacity of 66.66 mg g^{-1} was obtained from Langmuir isotherm. The pseudo-second-order kinetic model described the adsorption kinetics more accurately. Diffusion-based kinetics such as intraparticle diffusion and Bangham's model suggested that both film and intraparticle pore diffusion were involved in the adsorption process. The Elovich model pointed towards the chemisorption. The investigation of desorption and regeneration suggested that the material can be used as an effective sorbent for removal of Cd(II) from aqueous system.

Keywords Composite material · Cadmium (II) · Box–Behnken design · Adsorption · Kinetics · Isotherms

Introduction

The presence of heavy metals in the aquatic environment is of great concern worldwide. Cadmium(II) is considered as one of the most toxic elements which has high solubility and movability in aquatic systems. It is included in List 1 of the Dangerous Substances Directive of the European Union (Directive 2006/11/EC 2006). US Environmental Protection Agency has declared cadmium as a probable human carcinogen (IRIS 1999). It is often found in industrial wastewaters of rapidly growing industries such as Ni-Cd battery manufacturing, electroplating, pharmaceutical, tanneries, petroleum refining, pigment manufacturing, and pesticides (Mahmoud et al. 2016; Vekateswarlu and Yoon 2015). Cadmium(II) ion has the tendency to accumulate in living cells, and therefore affects the functioning of livers, lungs, kidneys, and cardiovascular systems (Bernard 2008). The irrigation of rice with river water containing Cd(II) led to the contamination of rice. The consumption of rice with high concentration of cadmium caused Itai-Itai disease in Japan (Rocha et al. 2009). The activity of enzymes is also prevented due to the combination of cadmium with sulfhydryl group in protein (Chen et al. 2008). World Health Organization (WHO) has recommended 3 μg L^{-1} cadmium as permissible limit in drinking water (WHO 2011). According to Central Pollution Control Board, India, the tolerance limits for Cd(II) in discharge into inland surface water and public sewer are 2.0 and 1.0 mg L^{-1}, respectively (IS

Responsible editor: Tito Roberto Cadaval Jr

Electronic supplementary material The online version of this article (https://doi.org/10.1007/s11356-018-2566-1) contains supplementary material, which is available to authorized users.

✉ Nafisur Rahman
nafisurrahman05@gmail.com

[1] Department of Chemistry, Aligarh Muslim University, Aligarh, UP 202002, India

10500, Drinking water specification 1992). In view of this, the removal of Cd(II) from wastewater is of great concern.

Literature survey revealed that several technologies such as chemical precipitation (Gavris et al. 2013; Lin et al. 2005), membrane separation (Ahamd et al. 2016), ion exchange (Wang et al. 2014), electrocoagulation (Heffron et al. 2016), ion floatation (Salmani et al. 2013), and adsorption (Rao et al. 2010) have been employed to remove Cd(II) ions from the water environment. Among them, adsorption process is considered as one of the most important technique because of easy operation, flexible in design, and reversible under certain experimental conditions. The advantage of adsorption method is the availability of large variety of adsorbents for the intended purpose, but some time, high cost of adsorbents increases the price of wastewater treatment. The performance of the adsorption process is directly related to the quality and selectivity of the adsorbent. Recently, agricultural waste materials such as rice husk (Hegazi 2013), black teawaste (Mohammed 2012), sugarcane bagasse (Garg et al. 2008), banana peels (Anwar et al. 2010), peanut shell (Xu and Zhuang 2014), barley hull (Maleki et al. 2011), pineapple waste (Mopoung and Kengkhetkit 2016), rice straw (Ding et al. 2012), and watermelon rind (Husein et al. 2017) have been considered as potential adsorbents for removal of Cd(II) from polluted water. In recent years, activated carbons have been used as adsorbents for removal of heavy metals. The adsorption capability and selectivity of activated carbons depends on the activation process and the materials from which they are produced. Activated carbons prepared from coffee residue (Boudrahem et al. 2011), doum palm shell (Gaya et al. 2015), *Cocos nucifera* (Hema and Srinivasan 2011), apricot stone (Kobya et al. 2005), madhucalongifolia fruit shell (Vilayatkar et al. 2016), municipal organic solid waste (Al-Malack et al. 2017), *Vitellaria paradoxa* shell (Jimoh et al. 2015), *Typha angustata* L. (Mohanapriya and Kumar 2016), *Tridax procumbens* (Singanan 2011), and wood of *Derris indica* (Venkatesan and Senthilnthan 2013) have shown potential to adsorb Cd(II) from aqueous solutions. The potential of magnetic nanocomposites has been exploited in the removal of heavy metals (Liu et al. 2013; Mehdinia et al. 2015). Hasanzadeh et al. have synthesized magnetic nanocomposite particles using iminodiacetic acid grafted poly(glycidylmethacrylate-maleicanhydride) copolymer (Hasanzadeh et al. 2017). The material showed high affinity for Cd(II) ions, and its adsorption capacity was 48.53 mg g^{-1}. Venkateswarlu and Yoon (2015) have developed water-dispersible diethyl-4-(4-amino-5-mercapto-4H-1,2,4-trizol-3-yl) phenyl phosphonate capped biogenic Fe_3O_4 magnetic nanocomposite which showed affinity for Cd(II). Magnetite nanoparticles with carboxymethyl-β-cyclodextrin was found to have properties that can selectively adsorb Cd(II) (Badruddoza et al. 2013). Manganese oxide-coated magnetic nanocomposite was prepared by a facile hydrothermal method which proved to be a good adsorbent for removal of Cd(II) (Kim et al. 2013). Magnetic iron oxide nanoparticles modified with 2-(5-bromo-2-pyridylazo)-5 diethylaminophenol showed affinity for Cd(II) with sorption capacity of 24.09 mg g^{-1} (Kakaei and Kazemeini 2016).

Recently, inorganic-organic hybrid composite materials have received considerable attention for their efficient application in the remediation of pollutants from aqueous systems. These materials have been developed by incorporation of organic components with variable functional groups into the inorganic matrix and thus providing superior rigidity, thermal stability, and selectivity (Rahman and Khan 2016; Rahman and Haseen 2014; Rahman and Haseen 2015). Tyrosine-containing inorganic-organic hybrid material contains -OH and -NH_2 groups in its framework and thus provides sites for selective interaction with metal ions (Kayan et al. 2014). An inorganic-organic hybrid material with N-(aminothioxomethyl)-2-thiophen carboxamide group provides selectivity towards Cu(II) and Cd(II), and its adsorption capacity for Cd(II) was 23.61 mg g^{-1} (Georgescu et al. 2013). A layered inorganic-organic hybrid material containing nitrogen and sulfur in the attached organic component proved to be an efficient adsorbent for adsorption of Cd(II) from water bodies (Dey et al. 2010). The literature survey revealed that hydrous zirconium oxide was exploited as adsorbent for removal of Cr(VI), Zn(II), Hg(II), and Cd(II) because the material possesses a rich amount of hydroxyl group which favors the inner sphere complexation with the target ionic species (Rodriguez et al. 2010; Mishra et al. 1996a; b; Mishra et al. 1997). However, the adsorption capacity of hydrous zirconium(IV) oxide for Cd(II) was low (Soenarjo and Wijaya 2006).

In classical method of experimental optimization, a large number of experiments were carried out using varying combinations of the variables to get the maximum response. Statistical experimental design such as response surface methodology (RSM) has eliminated the limitations of classical method by optimizing all the critical factors collectively (Cerrahoglu et al. 2017; Tak et al. 2015). RSM is an important statistical-based technique for evaluating the effects of several parameters simultaneously and thus providing the optimum conditions for desirable response (Tak et al. 2015). A mathematical model is also generated for prediction of response of a system under optimized conditions.

In the present study, a new composite material was prepared by incorporation of poly(o-phenylenediamine) into hydrous zirconium oxide which is expected to show selectivity for Cd(II). The analytical techniques such as fourier transform infrared spectroscopy (FTIR), X-ray diffraction (XRD), scanning electron microscopy (SEM) coupled with energy-dispersive X-ray spectroscopy (EDX), and thermogravimetric analysis-differential thermal analysis (TGA-DTA) have been used to characterize the material. Box–Behnken design

coupled with Derringer's desirability function was employed to optimize and examine the effects of contact time, solution pH, initial concentration of Cd(II) and adsorbent dose on the removal of Cd(II) from aqueous solution. The adsorption isotherms and kinetic features for the adsorption of Cd(II) onto the composite material have also been studied.

Experimental

Reagents

Poly(o-phenylenediamine)/hydrous zirconium oxide was prepared using the reagents such as o-phenylenediamine (98%, Loba Chemie Pvt. Ltd., India), ammonium peroxodisulphate (> 98%, Merck Specialities Pvt. Ltd., India), and zirconium oxychloride (99%, Otto Chemie Pvt. Ltd., India). Cadmium chloride (AR grade) was procured from Qualigens Fine Chemicals Pvt. Ltd., India.

Instruments

Atomic absorption spectrometer (Model GBC 932 Plus, GBC Scientific, Australia) was used to determine the concentration of metal ions in the solution. FTIR spectra were recorded with FTIR spectrophotometer (Perkin-Elmer Spectrum 2, UK). Simultaneous TGA-DTA were performed using DTG 60H thermal analyzer (Shimadzu, Japan) at the heating rate of 10 °C min^{-1}.

X-ray diffraction patterns of the material were obtained with XRD 1600 X-ray diffractometer (Shimadzu, Japan) using Cu Kα radiation ($\lambda = 1.5418$ Å). SEM images with EDX spectra were recorded with scanning electron microscope (JEOL JSM-6510LV, Japan). The surface area of PODA/HZO was determined by BET surface area analyzer (S.I. company Pvt. Ltd., India) using nitrogen atmosphere with degassing temperature of 80 °C. A water bath shaker (NSW Pvt. Ltd., India) was used to control temperature and shaking speed.

Preparation of poly-o-phenylenediamine/hydrous zirconium oxide (POPDA/HZO)

The composite material was prepared in three steps. In the first step, 1.4 g of o-phenylenediamine was dissolved in distilled water at room temperature. To this solution, 100 mL of 0.10 M ammonium persulfate was added at 10 °C and stirred for 30 min. The resulting mixture was kept for another 12 h at 10 °C, and finally, a brown colored poly-o-phenylenediamine gel was obtained. In the second step, the gel of hydrous zirconium oxide was obtained by mixing equal volumes of 6% ammonium hydroxide and 0.10 M $ZrOCl_2.8H_2O$ solutions. Lastly, poly(o-phenylenediamine)/hydrous zirconium oxide composite material was prepared by mixing both the gels with constant stirring on a magnetic stirrer for 6 h at 30 °C, and then, the resulting slurry was kept for another 24 h. It was filtered, and adhering impurities were removed by washing with distilled water. After drying in an oven at 50 °C, the material was placed in distilled water to get small granules. Further, it was sieved to obtain particles of uniform size (50–100 μm). The synthesis of POPDA/HZO is shown in Scheme 1.

Batch adsorption experiments

The adsorption of Cd(II) ions onto POPDA/HZO composite was studied in batch mode. The adsorption experiments were performed by equilibrating the different amounts of adsorbent with varying concentrations of Cd(II), pH, and contact time at a fixed temperature. In general, a known mass of the adsorbent with 20 mL of each Cd(II) ions solution, adjusted to a known pH, was agitated on a shaker for a given contact time. After separation of the adsorbent from the solution, Cd(II) concentration in the solution was determined by atomic absorption spectroscopy (AAS). The percentage removal of Cd(II) and adsorption capacity of POPDA/HZO can be obtained from the following equations:

$$\text{Removal efficiency}\ (\%) = \frac{C_0 - C_e}{C_0} 100 \quad (1)$$

$$q_e = \frac{(C_0 - C_e)V}{M} \quad (2)$$

where q_e is experimental adsorption capacity (mg g^{-1}). C_0 and C_e are the initial and equilibrium concentrations (mg L^{-1}) of Cd(II) in the liquid phase, respectively. M and V are the mass of adsorbent (g) and volume of solution (L), respectively.

Box–Behnken experimental design

The optimization of major operating parameters for Cd(II) removal was carried out using Box–Behnken design technique under response surface methodology (Zhang et al. 2017). To study the influence of operating parameters on the Cd(II) removal efficiency, four variables, each at three levels, were selected: contact time (A), initial pH of solution (B), adsorbent dose (C), and initial concentration of Cd(II) (D) which are shown in Table 1. The experimental runs required under Box–Behnken design can be calculated using the equation (Jain et al. 2011):

$$N = k^2 + k + C_p \quad (3)$$

where k is the factor number and Cp is the replicate number of central point. Therefore, a total of 29 experiments have been carried out under four-factor and three-level design. The actual experimental design matrix is given in Table 2. RSM uses the data obtained from experimental design to optimize the

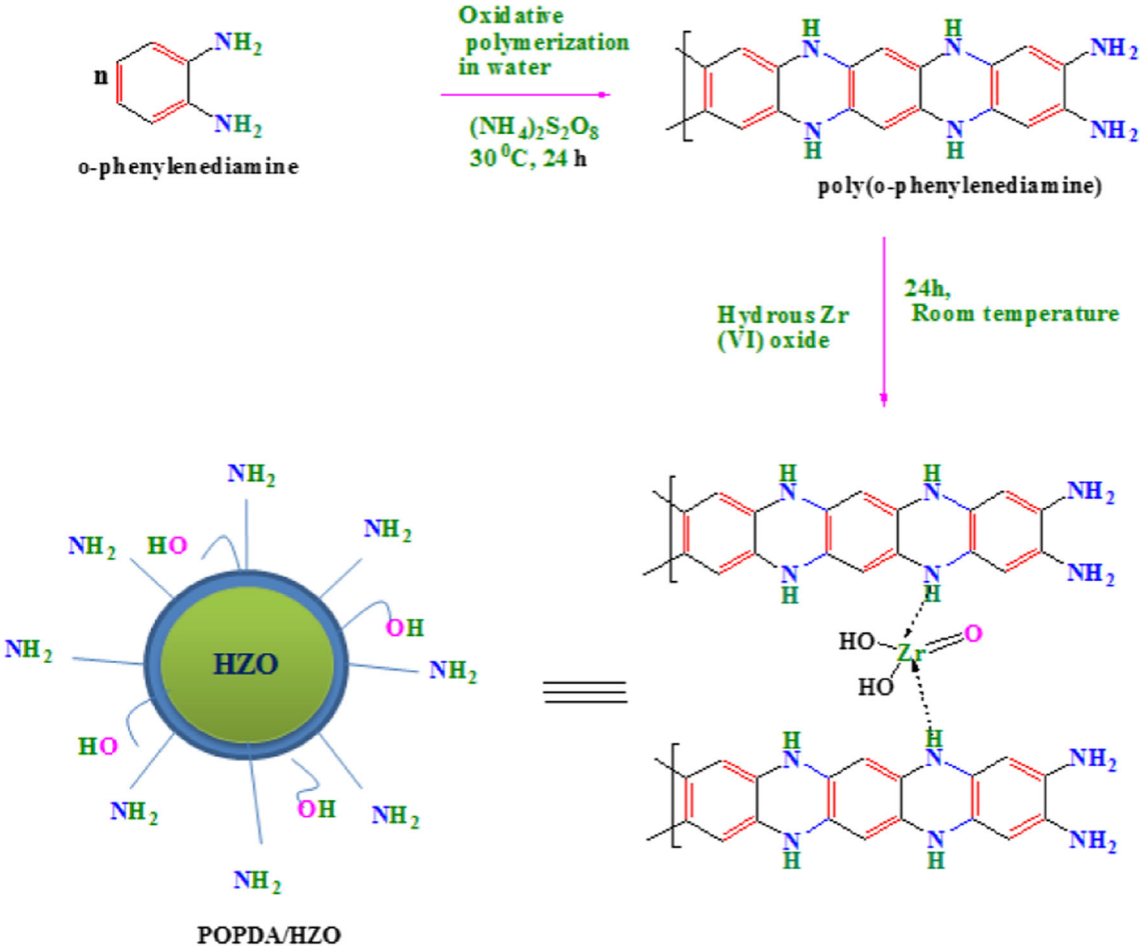

Scheme 1 Synthesis of POPDA/HZO

variables for the adsorption process. Fitting and analysis of data obtained from experimental design followed the second-order polynomial model. The general form of second-order polynomial model for response surface analysis is expressed as follows (Rahmanidn et al. 2012):

$$Y = \beta_0 + \sum_{i=1}^{k} \beta_i X_i + \sum_{i=1}^{k} \sum_{j=1}^{k} \beta_{ij} X_i X_j + \sum_{i=1}^{k} \beta_{ii} X_i^2 \quad (4)$$

where Y is the predicted response (% removal); X_i and X_j are the coded values of independent variables; and β_0, β_i, β_{ii}, and β_{ij} are the regression coefficients for the intercept, linear, quadratic, and interaction terms, respectively. Data were processed for Eq. (4) using Design Expert program (free trial 10.0.7.0 version).

Table 1 Independent variables and their levels used for Box–Behnken design

Variables	Unit	Factors	Range and level coded values		
			(− 1)	0	(+ 1)
Time	min	A	10	45	80
pH	–	B	3	6	9
Dosage	mg	C	10	25	40
Concentration	mg L^{-1}	D	30	50	70

Desirability function

The modified desirability function approach (Derringer and Suich 1980) was used to evaluate the optimum values of input variables for obtaining the optimum performance levels for one or more responses. During the optimization procedure, each response (Y_i) is changed into individual desirability function (d_i) that varies between 0 and 1, indicating towards undesirable response ($d_i = 0$) and completely desirable response ($d_i = 1$). The intermediate values of d_i pointed towards more or less desirable responses.

Different desirability functions may be developed for a response Y_i which is to be maximized, minimized, or assigned a target value within an acceptable range of response values. The range of response is given by (β-α) where β and α are the highest and lowest values of response, respectively. In order to maximize the response, the individual desirability index can be calculated using the following equation (Candioti et al. 2014):

Table 2 Box–Behnken design matrix and experimental and predicted values (response) of Cd(II) removal (%) by POPDA/HZO

Experimental	Independent variables				Response	
Run	A: Time min	B: pH	C: Dosage mg 20 mL^{-1}	D: Concentration mg L^{-1}	Actual removal %	Predicted removal %
1	10	6	40	50	39.76	41.19
2	45	9	25	30	99.6	93.41
3	10	6	25	70	30.76	36.31
4	45	9	40	50	99.6	104.72
5	45	6	40	30	99.6	93.33
6	80	6	10	50	63.08	62.80
7	80	6	40	50	99.6	104.64
8	10	9	25	50	39.76	39.27
9	45	6	25	50	99.6	99.6
10	45	6	25	50	99.6	99.6
11	45	6	10	70	52.08	56.99
12	45	3	25	70	38.14	45.47
13	80	6	25	70	95.21	89.03
14	45	6	10	30	63.08	67.83
15	45	6	25	50	99.6	99.6
16	10	3	25	50	25.37	16.39
17	45	9	10	50	63.08	62.521
18	45	9	25	70	95.21	89.69
19	10	6	25	30	39.76	46.15
20	45	3	25	30	50.14	56.80
21	45	3	10	50	40.41	35.40
22	45	3	40	50	50.14	50.91
23	10	6	10	50	29.32	25.42
24	45	6	25	50	99.6	99.6
25	45	6	25	50	99.6	99.6
26	80	6	25	30	99.6	95.26
27	80	3	25	50	50.14	49.27
28	45	6	40	70	95.21	89.11
29	80	9	25	50	99.6	107.22

$$d_i = \begin{bmatrix} 0 & if\, Y_i < \propto \\ \left(\frac{Y_i - \propto}{\beta - \alpha}\right)^p & if \propto \le Y_i \le \beta \\ 1 & if\ Y_i > \beta \end{bmatrix} \quad (5)$$

where p is the power value named "weight" which is set to determine how important it is for predicted response to be close to the maximum.

Equation (6) is used to calculate the d_i when the response Y_i is to be minimized.

$$d_i = \begin{bmatrix} 1 & if\, Y_i < \propto \\ \left(\frac{\beta - Y_i}{\beta - \alpha}\right)^q & if \propto \le Y_i \le \beta \\ 0 & f\ Y_i > \beta \end{bmatrix} \quad (6)$$

where q is the weight for determining how important it is for the response to be close to the minimum.

Finally, Eq. (7) describes the individual desirability function when a target value T_i is the most desired response.

$$d_i = \begin{bmatrix} 0 & if\, Y_i < \propto \\ \left(\frac{Y_i - \propto}{T_i - \alpha}\right)^q & if \propto < Y_i < \beta \\ 1 & Y_i = T_i \\ \left(\frac{Y_i - \beta}{T_i - \beta}\right)^q & if\, T_i < Y_i < \beta \\ 0 & if\ Y_i > \beta \end{bmatrix} \quad (7)$$

The overall desirability function, D, is obtained by combining individual desirability function to achieve the best joint responses using the following equation:

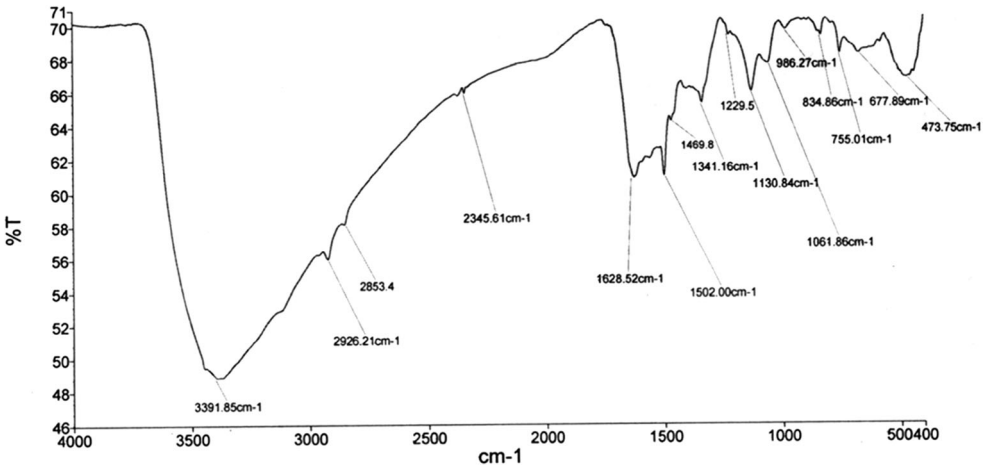

Fig. 1 FTIR spectrum of POPDA/HZO

$$D = (d_1 \times d_2 \times \ldots\ldots \times d_m)^{1/m} \quad (8)$$

where m is the number of responses.

Kinetic studies

For kinetic studies, 25 mg of the adsorbent was agitated with 20 mL of Cd(II) solution (50 mg L^{-1}, pH 6) in Erlenmeyer flask on a shaker at a constant temperature (30, 40, or 50 °C). The adsorbent was separated from the solution at time intervals of 5, 10, 15, 20, 25, 30, 35, 40, and 45 min, and the concentration of Cd(II) ions was determined by AAS.

Error analysis

Statistical analysis was carried out to judge the fitness of adsorption isotherm and kinetic equations to the experimental data. For this purpose, values of chi-square (χ^2) and average percentage error (APE) were calculated using the following equations:

$$\chi^2 = \sum_{i=1}^{n} \frac{\left(q_{e,exp} - q_{e,cal}\right)^2}{q_{e,exp}} \quad (9)$$

$$\mathrm{APE}(\%) = \frac{\sum_{i=1}^{N} \left| \left(q_{e,exp} - q_{e,cal}\right)/q_{e,exp} \right|}{N} \quad (10)$$

where $q_{e,exp}$ and $q_{e,cal}$ are experimental capacity data and capacity determined from a model, respectively. The values of χ^2 and APE will be smaller when the experimental capacity is close to the capacity computed from a model.

Desorption and regeneration

To study the desorption, a known amount of Cd(II) sorbed POPDA/HZO was treated with 0.2 M NaOH for about 20 min, and finally, the adsorbent was separated from liquid phase. Atomic absorption spectrometer was used to determine the Cd(II) released in the liquid phase. The regeneration was tested by performing adsorption-desorption processes several times using the same adsorbent.

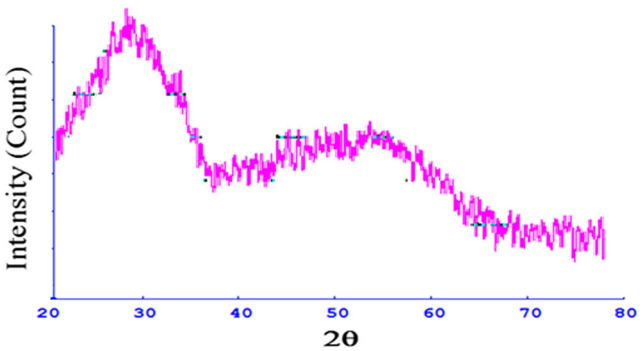

Fig. 2 XRD pattern of POPDA/HZO

Results and discussion

Physiochemical characterization of hybrid material

FTIR spectrum of HZO (Fig. S1) shows that broad absorption band between 3000 and 3600 cm^{-1} peaking at 3402 cm^{-1} is assigned to stretching vibration of O-H bands of coordinated water. The absorption band peaking at 1627 cm^{-1} is due to H-O-H bending vibration (Nakamoto 2009). The absorption peak at 1580 cm^{-1} indicates the vibration of Zr-OH (Dou et al. 2012). Another band peaking at 1400 $cm^{-1}$is attributed to the characteristic O-H bending vibration from Zr-OH (Zong et al. 2013). The absorption bands peaking at 849, 666, and

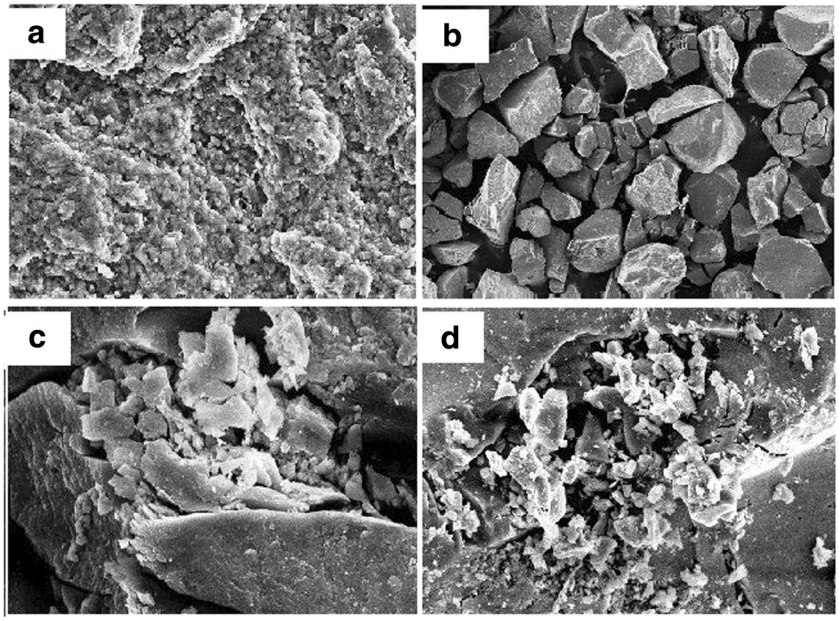

Fig. 3 SEM images of **a** HZO, **b** POPDA, **c** POPD/HZO, and **d** Cd-loaded POPD/HZO

473 cm^{-1} indicated the lattice vibration of Zr-O (Ali and Zaki 1998; Seredych and Bandosz 2010).

The FTIR spectrum of POPD/HZO (Fig. 1) shows that broad absorption band centered at 3391 cm^{-1} is attributed to free N-H stretching vibration which indicated the presence of secondary amino groups (-N-H-) (Huang et al. 2001). The stretching vibration of O-H bands of coordinated water is also overlapping in this region. Two strong peaks centered at 1628 and 1502 cm^{-1} are ascribed to aromatic C=C stretching vibrations (Socrates 1980). The strong peak at 1628 cm^{-1} is also indicative of N-H deformation vibrations associated with primary aromatic amine and bending vibration due to H-O-H (Socrates 1980). The weak band at 1469 cm^{-1} pointed towards aromatic ring C=C stretching. The absorption band observed at 1341 cm^{-1} is the result of C-N stretching vibrations, confirming the presence of both primary and secondary aromatic amines (Socrates 1980). The bands appearing at 834 and 755 cm^{-1} are due to C-H out of plane deformation of benzene nuclei (Ichinohe et al. 1998). FTIR spectrum also exhibits two bands at 1130 and 1061 cm^{-1} which can be attributed to aromatic =C-H in-plane deformation vibration. The lattice vibration of Zr-O can be characterized by the peaks at 834, 677, and 473 cm^{-1}.

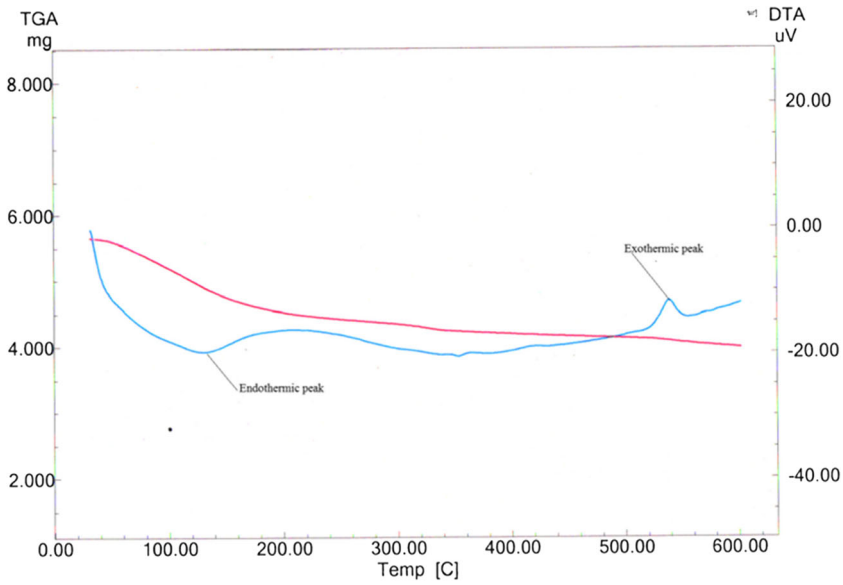

Fig. 4 TGA and DTA curves of PODA/HZO

Table 3 Results of ANOVA and percentage contribution of the components for the quadratic model

Source	Sum of squares	*df*	Mean square	*F* value	*p* value Prob > *F*		VIF	PC
Model	22,326.99	14	1594.79	33.72	< 0.0001	Significant		
A-Time	7625.52	1	7625.52	161.23	< 0.0001		1.00	34.15
B-pH	4900.93	1	4900.93	103.62	< 0.0001		1.00	21.95
C-Dosage	2490.05	1	2490.05	52.65	< 0.0001		1.00	11.15
D-Concentration	170.03	1	170.03	3.59	0.0788		1.00	0.76
AB	307.48	1	307.48	6.50	0.0231		1.00	1.138
AC	170.04	1	170.04	3.60	0.0788			0.76
AD	5.31	1	5.31	0.11	0.7425			0.024
BC	179.43	1	179.43	3.79	0.0718			0.80
BD	14.48	1	14.48	0.31	0.5888			0.064
CD	10.92	1	10.92	0.23	0.6382			0.05
A^2	4294.96	1	4294.96	90.81	< 0.0001		1.08	19.04
B^2	2813.96	1	2813.96	59.50	< 0.0001		1.08	12.60
C^2	1529.77	1	1529.77	32.34	< 0.0001		1.08	6.85
D^2	357.93	1	357.93	7.57	0.0156		1.08	1.60
Residual	662.16	14	47.30					
Lack of fit	662.16	10	66.22					
Pure error	0.000	4	0.000					
Cor total	22,989.15	28						
Fit statistics								
R^2							0.9712	
Goodness of fit R^2							0.9429	
Goodness of prediction R^2							0.8557	

PC percentage contribution

Figure 2 shows the XRD analysis of POPDA/HZO. Two broad peaks at 2θ of 30° and 56° were observed corresponding to d-spacing of 2.978 and 1.6422 Å, respectively, which suggested towards the amorphous nature of the material. The SEM image (Fig. 3a) of HZO showed the irregular surface morphology due to agglomeration of particles of varying shape and size and also pointing towards its porous nature. Similar observations for HZO have been reported earlier (Rahman et al. 2015). The SEM image of POPDA (Fig. 3b) exhibited rugged surface consisting of particles of different sizes and shapes and also showing void spaces between particles. The incorporation of POPDA into HZO caused a change in surface morphology (Fig. 3c). It is also evident from Fig. 3c that surface of the composite is covered by the POPDA. The SEM image (Fig. 3d) of Cd(II) sorbed POPDA/HZO is similar to that of the parent composite material. The EDX spectrum of POPDA/HZO (Fig. S2) showed the presence of Zr (40.7%), C (39.8%), N (13.37%), and O (6.25%). The results of SEM-EDX demonstrated that the immobilization of POPDA has taken place on HZO matrix. The EDX spectrum of Cd(II) sorbed POPDA/HZO revealed the successful adsorption of Cd(II) onto the composite material. The BET surface area of POPDA/HZO was found to be 332.1 $m^2\ g^{-1}$.

POPDA/HZO composite material was characterized by TGA and DTA in the temperature range 30 to 600 °C (Fig. 4). It was observed that the weight loss occurred in three steps. In the first transition stage, the weight loss (15.85%) occurred in the temperature interval of 30 to 150 °C, which can be attributed to removal of interstitial water (Gupta et al. 2005; Singh et al. 2003). The second stage of thermal transition was observed from 150 to 400 °C. During this stage, the weight loss was 11.76% which is due to the removal of $-NH_2$ groups and degradation of organic moiety of the composite material (Samanta et al. 2017). In the third stage, the weight loss (3.53%) was observed in the temperature range of 400 to 560 °C. This weight loss may be due to the decomposition of polymer chain (Muthirulan et al. 2013). Above 560 °C, the weight becomes constant due to formation of zirconium oxide. The DTA curve showed two broad endothermic peaks centered at 131 and 345 °C. The first peak indicated the loss of water molecules the second broad band suggested the removal of substituted groups. An exothermic peak was observed at 539 °C, conforming the degradation of organic molecule.

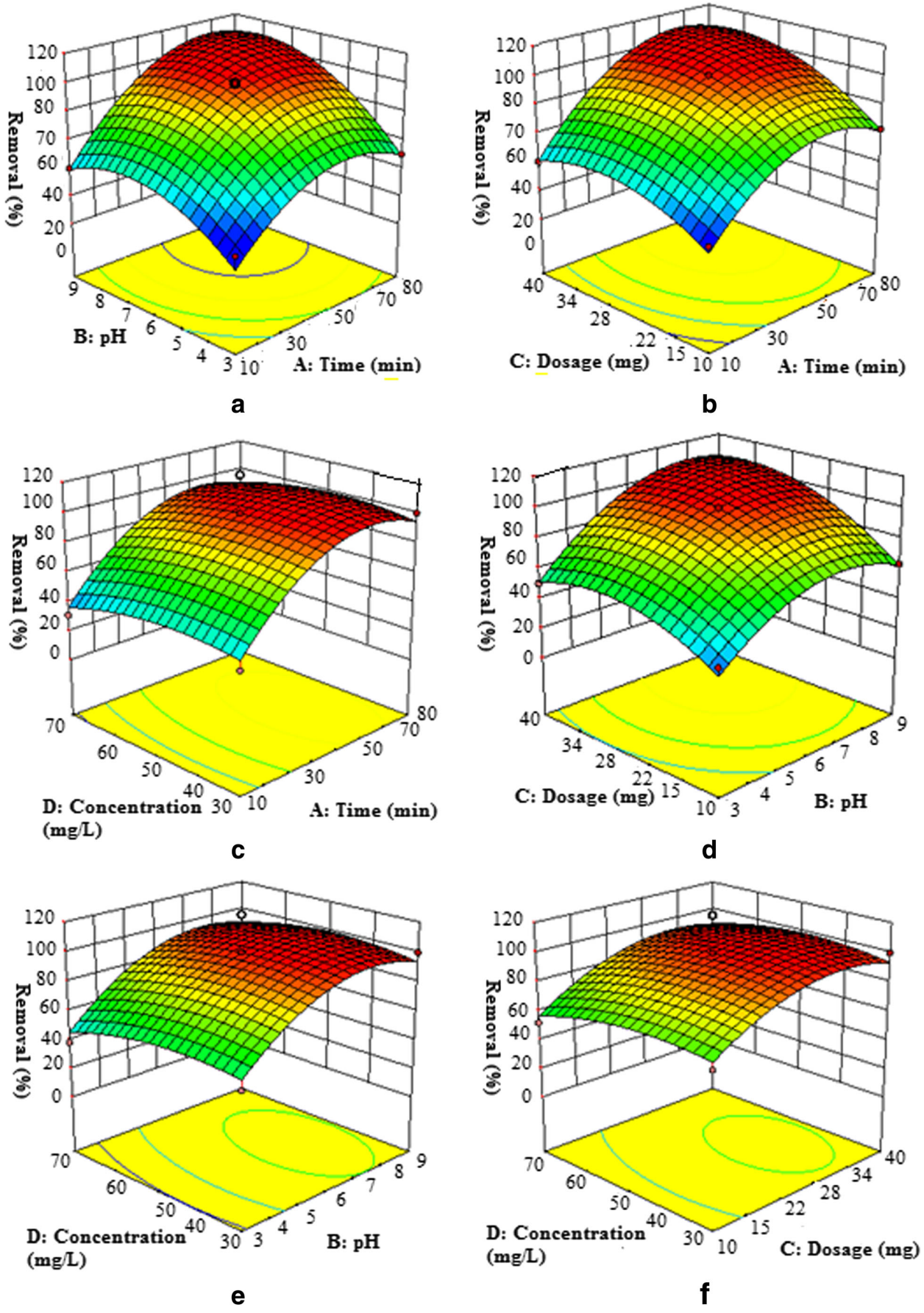
Removal (%)
120
100
80
70
60
40
20
0
B: pH
9
8
7
6
5
4
3
A: Time (min)
10
30
50
70
80
a
C: Dosage (mg)
40
34
28
22
15
10
b
D: Concentration (mg/L)
70
60
50
40
30
c
d
e
f

◀ **Fig. 5** Response surface plots for the percent removal of Cd(II) versus (**a**) pH and contact time, (**b**) adsorbent dose and contact time, (**c**) initial concentration and contact time, (**d**) adsorbent dose and pH, (**e**) initial concentration and pH, and (**f**) initial and adsorbent dose

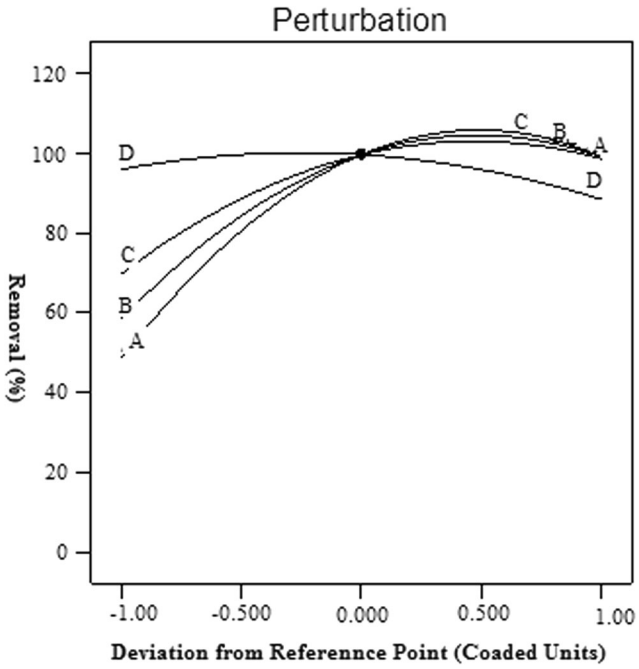

Fig. 6 Perturbation plots for percent removal of Cd(II) by POPDA/HZO

Box–Behnken statistical analysis

The experimental data obtained from Box–Behnken design were fitted to linear, interactive, quadratic, and cubic models to generate the regression equations. The suitability of models to describe the removal of Cd(II) by POPDA/HZO was judged by comparing the sequential model sum of squares and model statistics (Table S1). The quadratic model was selected on the basis of high F value, lower p value (< 0.0001) and minimum predicted residual sum of squares (PRESS) for further analysis. Therefore, an empirical relationship between the predicted response (% removal) and independent variable can be represented by the following quadratic model.

Equation in terms of coded factors:

$$\text{Removal}\ (\%) = +99.60 + 25.21\text{A} + 20.21\text{B} + 14.41\text{C} - 3.76\text{D} + 8.77\text{AB} + 6.52\text{AC} + 1.15\text{AD} + 6.70\text{BC} + 1.90\text{BD} + 1.65\text{CD} - 25.73\text{A}^2 - 20.83\text{B}^2 - 15.36\text{C}^2 - 7.43\text{D}^2 \quad (11)$$

Equation in terms of actual factors:

$$\text{Removal}\ (\%) = -123.819 + 1.717 * \text{Time} + 25.444 * \text{pH} + 2.646 * \text{Dosage} + 1.267 * \text{Concentration} + 0.084 * \text{Time} * \text{pH} + 0.013 * \text{Time} * \text{Dosage} + 1.646\text{E} - 003 * \text{Time} * \text{Concentration} + 0.149 * \text{pH} * \text{Dosage} + 0.032\ \text{pH} * \text{Concentration} + 5.508\text{E} - 003 * \text{Dosage} * \text{Concentration} - 0.021 * \text{Time}^2 - 2.314 * \text{pH}^2 - 0.068\ \text{Dosage}^2 - 0.019 * \text{Concentration}^2 \quad (12)$$

The analysis of variance (ANOVA) was applied to ensure the significance and adequacy of the model. The results of ANOVA and test for the significance of the regression model are summarized in Table 3. The F value for the model (33.72) is greater than that obtained from the standard distribution table (2.47 at 95% confidence level) which demonstrated the significance of the model. The prob > F value for the model is lower than 0.05 (95% confidence level) which further suggested that the model is statistically significant. The lack-of-fit test suggested that the selected model has insignificant lack-of-fit. Moreover, the high correlation coefficient value ($R^2 = 0.9712$) demonstrated a good fit between the predicted response and experimental data points (Fig. S3). The value of variance inflation factor (VIF) (Table 3) for all the variables (A, B, C, and D) is 1.0. This demonstrated that there is no correlation among kth predictor and the remaining predictor variables. Therefore, the variance is not inflated at all. The VIF value for A^2, B^2, C^2, and D^2 is 1.08 which indicated the existence of a very low level of multicollinearity. Further, the normal probability plot of residual (Fig. S4) was used to check the goodness of fit of the quadratic model. As can be seen in Fig. S4, the data points lie reasonably close to a straight line, confirming the adequacy of the quadratic model. The values of adjusted R^2 and predicted R^2 should be within 0.20 of each other to define the reasonable agreement (Mourabet et al. 2012). In this study, the values of goodness of fit (R^2) and goodness of prediction (R^2) were 0.9424 and 0.8557, respectively, which suggested a reasonable agreement between them and confirming the adequacy of the quadratic model.

Effect of variables and response surface plots

The percentage contribution (PC) of each variable in the response model can be calculated using the following expression (Bandari et al. 2015):

$$PC = \frac{SS_i}{SS_m}\,100 \quad (13)$$

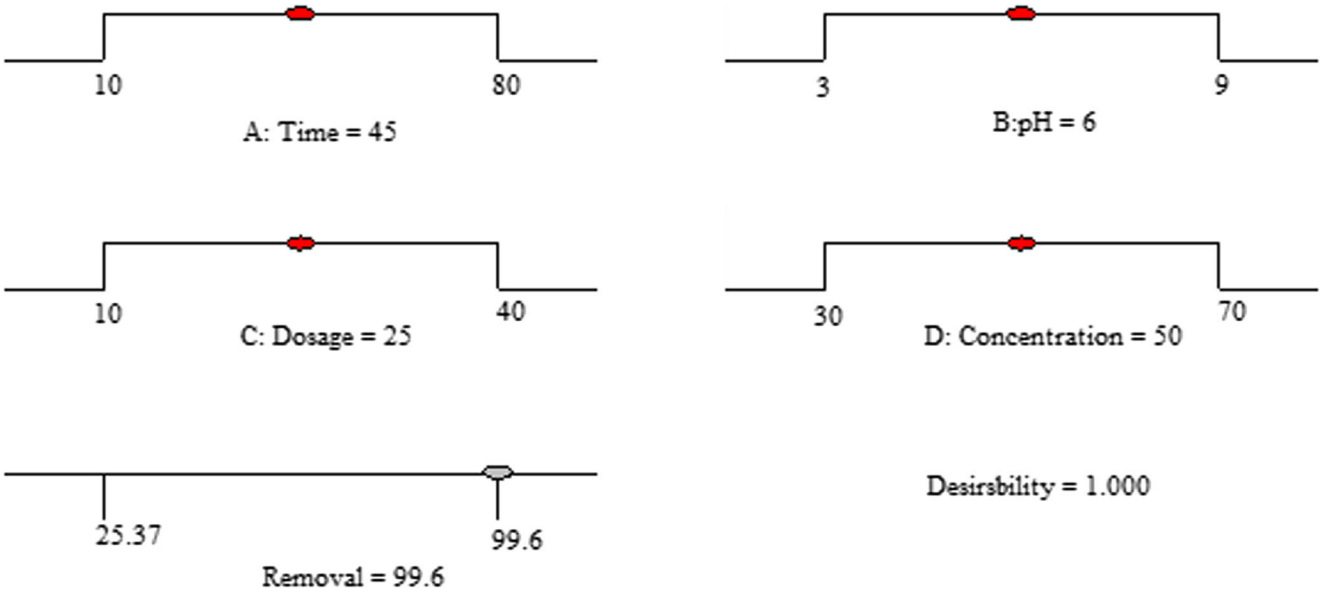

Fig. 7 Profiles for the predicted response and desirability functions for the percent removal of Cd(II)

where SS_i and SS_m are the sum of squares for the individual variable and sum of squares for the model. The results are summarized in Table 3. The results revealed that the contact time, initial pH of solution, and adsorbent dose have exhibited high levels of contribution in the removal of Cd(II) by POPDA/HZO with PC values of 34.15, 21.95, and 11.15, respectively. The contribution of initial concentration of Cd(II) is minimum (0.76%) in the response model. The interactive term AB showed PC value of 1.38, whereas all other interactive terms have contributed to a smaller extent in the removal of Cd(II).

RSM in combination with Box–Behnken design is employed to optimize the variables for obtaining the maximum removal of Cd(II) by POPDA/HZO. The three-dimensional response surface plots were obtained for a given pair of variables while keeping other factors constant. Figure 5a shows the interactive effect of pH and contact time on the removal of Cd(II). As can be seen in the figure that at any fixed pH, the removal of Cd(II) increases with contact time and the maximum removal (99.6%) was achieved at a contact time of 45 min. The interaction of adsorbent dose with contact time and their relation to percentage removal of Cd(II) at pH 6 and initial concentration of 50 mg L^{-1} is shown in Fig. 5b. It is evident from the Fig. 5b that the removal efficiency increases with increase in both adsorbent dose and contact time. This is due to the fact that the greater amounts of POPDA/HZO could provide increased surface area and more active sites for binding with the Cd(II) ions.

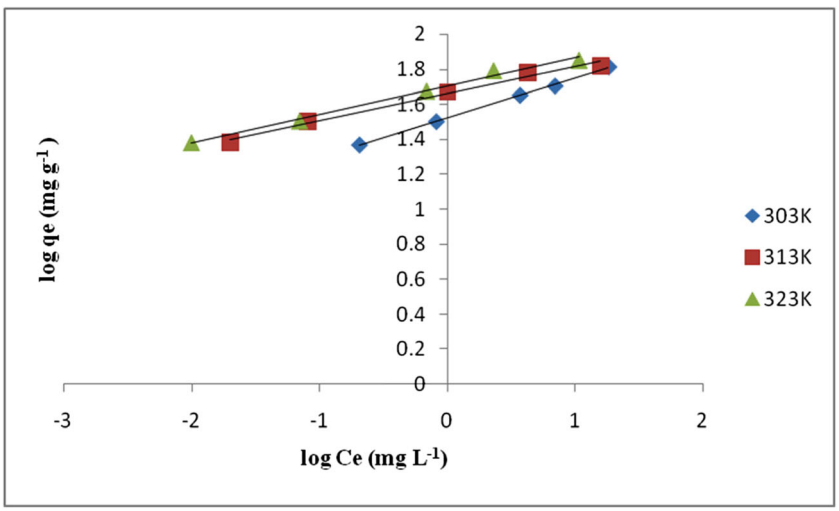

Fig. 8 Freundlich isotherm plots for the adsorption of Cd(II) onto POPDA/HZO

Table 4 Isotherm parameters, regression coefficient and error functions obtained by linear fitting for adsorption of Cd(II) onto POPDA/HZO (C_0 10–100 mg L^{-1}, adsorbent dose 1.25 g L^{-1}, contact time 45 min, pH 6)

Isotherm	Temperature (K)	Parameters				Error function	
Langmuir		q_m (mg g^{-1})	K_L (L mg^{-1})		R^2	APE	χ^2
	303	66.66	2.14		0.998	2.00	0.026
	313	71.42	4.66		0.998	5.81	5.810
	323	76.92	6.57		0.990	7.71	0.425
Freundlich		q_m[a] (mg g^{-1})	n	K_F	R^2	APE	χ^2
	303	64.26	3.75	33.41	0.999	1.60	0.017
	313	68.04	6.45	45.60	0.998	1.13	0.008
	323	71.44	6.13	50.46	0.997	0.05	0.000
Temkin		q_m (mg g^{-1})	A_T (10^3)	B_T	R^2	APE	χ^2
	303	64.06	0.35	7.38	0.917	1.96	0.025
	313	64.50	25.28	4.99	0.939	4.10	0.111
	323	70.42	1.95	7.07	0.979	1.37	0.013
Dubinin-Radushkevich		q_m (mg g^{-1})	K_{ad} (10^{-8})		R^2	APE	χ^2
	303	53.03	2		0.588	18.85	2.322
	313	56.59	0.9		0.881	15.82	1.678
	323	57.22	0.6		0.818	19.87	2.819

[a] The experimental values of adsorption capacity (q_e) for Cd(II) are 65.35, 67.27, and 71.41 mg g^{-1} at 303, 313, and 323 K, respectively

The plot (Fig. 5c) for combined effect of initial concentration and contact time at constant pH (6) and adsorbent dose (25 mg 20 mL^{-1}) revealed that at any fixed contact time, the removal percentage increases with increasing solution concentration. Above 50 mg L^{-1}, percentage removal of Cd(II) decreases due to nonavailability of sufficient number of active sites for interaction with Cd(II).

Figure 5d shows the combined effect of pH and adsorbent dose on the uptake of Cd(II) by POPDA/HZO. It was observed that the removal efficiency increased with increasing amount of adsorbent at any given pH value. Moreover, at pH < 6, the removal efficiency decreases, which may be due to protonation of -NH_2 group present in POPDA and Zr-OH_2^+. At pH 6–9, -NH_2 group is freely available for binding with the Cd(II), and thus exhibiting the maximum removal in this pH range. It was also observed that the percent removal of Cd(II) increases from 16.39 to 99.96% from pH 3 to 6.

Figure 5e shows the combined effect of pH and initial concentration on the removal of Cd(II). The experimental results revealed that the percent removal increases with increase in pH up to 6 when the initial concentration was 50 mg L^{-1}. Above this concentration (i.e., > 50 mg L^{-1}), percentage removal of Cd(II) decreases due to nonavailability of sufficient number of active sites for

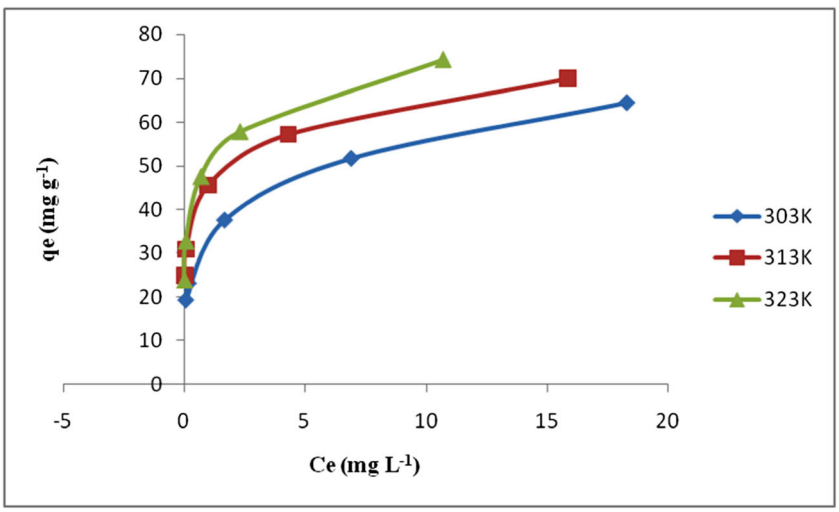

Fig. 9 Nonlinear Freundlich isotherm plots for the adsorption of Cd(II) onto POPDA/HZO

Table 5 Isotherm parameters, regression coefficient, and error functions obtained by nonlinear fitting for the adsorption of Cd(II) onto POPDA/HZO (C_0 10–100 mg L^{-1}, adsorbent dose 1.25 g L^{-1}, contact time 45 min, pH 6)

Isotherm	Temperature (K)	Parameters				Error function	
Langmuir		q_m [a](mg g^{-1})	K_L (L mg^{-1})		R^2	APE	χ^2
	303	65.939	2.14		0.960	0.80	0.005
	313	70.469	4.66		0.949	4.75	0.152
	323	75.835	6.57		0.949	6.196	0.274
Freundlich		q_m (mg g^{-1})	n	K_F	R^2		
	303	65.470	3.75	33.41	0.979	0.18	0.000
	313	70.020	6.45	45.60	0.981	4.05	0.110
	323	74.299	6.13	50.46	0.981	3.90	0.109
Temkin		q_m (mg g^{-1})	A_T (10^3)	B_T	R^2		
	303	65.682	0.35	7.38	0.977	0.508	0.001
	313	70.251	25.28	4.99	0.978	4.431	0.132
	323	74.827	1.95	7.07	0.978	4.785	0.163

[a] The experimental values of adsorption capacities (q_e) of cadmium are 65.35, 67.27, and 71.41 mg g^{-1} at 303, 313, and 323 K temperature, respectively

interaction with Cd(II). The interactive effect of adsorbent dose and initial concentration is shown in Fig. 5f. At lower amount of adsorbent dose, the removal efficiency decreased owing to the nonavailability of sufficient active sites for interaction with the Cd(II) ions.

Interactive effects of four variables

The perturbation graph is commonly used to study the interactive effects of all variables at a time. The perturbation plot (Fig. 6) shows the percent removal of Cd(II) as a function of

Table 6 Kinetic parameters for adsorption of Cd(II) onto POPDA/HZO

Kinetics	Temperature (K)		Parameters		
			$q_{e,cal}$ [a] (mg g^{-1})	$K1$	R^2
Pseudo-first-order	303		31.08	0.039	0.925
	313		33.02	0.055	0.824
	323		35.12	0.056	0.968
			$q_{e,cal}$ (mg g^{-1})	$K2$	R^2
Pseudo-second-order	303		47.46	0.008	0.997
	313		48.66	0.007	0.997
	323		49.96	0.006	0.998
			∝	β	R^2
Elovich model	303		176.97	0.19	0.991
	313		177.79	0.18	0.985
	323		213.89	0.15	0.974
			C_{id}	K_{id}	R^2
Intraparticle diffusion model	303	I	16.29	4.65	0.980
		II	28.30	1.36	0.988
	313	I	16.29	4.65	0.980
		II	33.70	0.65	0.995
	323	I	15.53	5.06	0.995
		II	34.41	0.42	0.987
		K_0		∝	R^2
Bangham's equation	303	9.917		0.386	0.961
	313	9.894		0.394	0.962
	323	10.219		0.389	0.957

[a] The experimental values of adsorption capacity (q_e) are 49.52, 49.67, and 49.90 mg g^{-1} at 303, 313, and 323 K, respectively, when $C_0 = 50$ mg L^{-1}

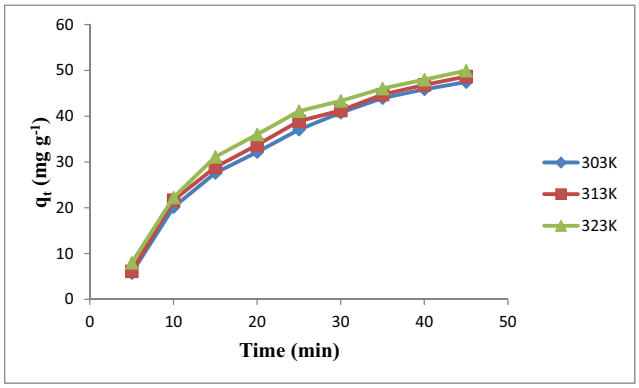

Fig. 10 Pseudo-second-order kinetic plots for the adsorption of Cd(II) onto POPDA/HZO

each variable moving from the lowest coded value while all other variables kept constant at the center point of the design (coded zero level). As can be seen in Fig. 6, the factors such as contact time, initial pH, and adsorbent dose have pronounced effect on the removal of Cd(II) The flat curve for initial concentration indicated that the removal is less affected by this variable. Similar observations were also reported for the adsorption of Cd(II) using trichodermaviride as adsorbent (Singh et al. 2010).

Optimization of variables

In order to study numerical optimization, a minimum and a maximum level must be given for each input variable whereas the response was designed to obtain the maximum. The results presented in Fig. 7 demonstrated the ranges of input variables obtained from the model. Response surface methodology with desirability function has predicted the optimum values for each independent variables for achieving the maximum removal (99.6%) of Cd(II). The optimum values of variables are as follows: contact time = 45 min, initial pH of solution = 6, adsorbent mass = 25 mg 20 mL^{-1}, and initial concentration of Cd(II) ions = 50 mg L^{-1}. The confirmatory experiments were also carried out under the optimized conditions which agreed well with the predicted value.

Equilibrium modeling

The experimental equilibrium data for adsorption of Cd(II) onto POPDA/HZO were examined using Langmuir, Freundlich, Temkin, and Dubinin-Radushkevich isotherm models. The linear and nonlinear equations of the above models are given in Table S2.

Linear fitting of isotherm models

The linear plots for Freundlich isotherm model is shown in Fig. 8. The plots for Langmuir, Temkin, and Dubinin-Radushkevich (D-R) isotherm models are shown in Figs. S5, S6, and S7, respectively. The isotherm parameters for each model were calculated from corresponding isotherm plots and summarized in Table 4. In addition, the separation factor, R_L, was calculated from the K_L values of Langmuir model to examine the types of isotherm (Talebi et al. 2017; Tehrani et al. 2017) and is defined as follows:

$$R_L = \frac{1}{1 + k_L C_o} \tag{14}$$

where C_0 is the initial concentration of Cd(II) ions (mg L^{-1}). The adsorption process is considered favorable when $0 > R_L < 1$. In the present study, the values of R_L were found to be less than unity at all concentrations (10–100 mg L^{-1}) and temperatures (303, 313, and 323 K) (Fig. S8). This demonstrated that the adsorption of Cd(II) onto POPDA/HZO is a favorable process. The mean free energy, E (kJ mol^{-1}), was calculated from K_d values (Dubinin-Radushkevich isotherm constant) using the following equation:

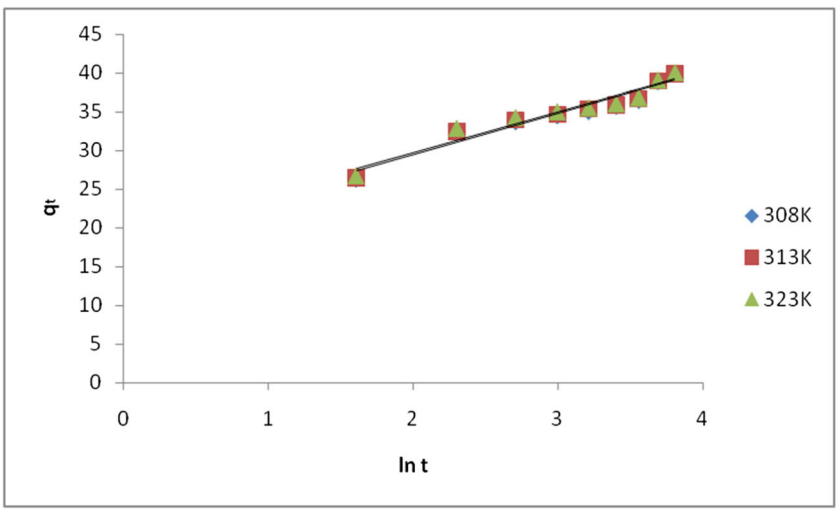

Fig. 11 Elovich plots for the adsorption of Cd(II) onto POPDA/HZO

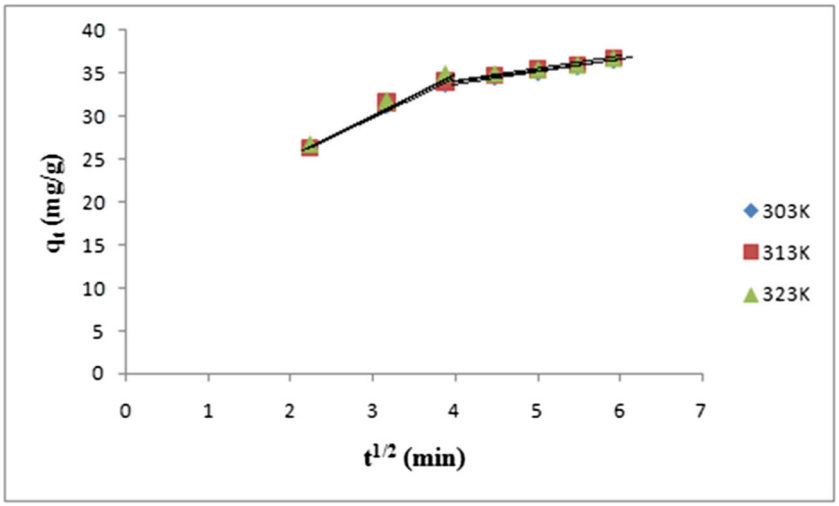

Fig. 12 Intraparticle diffusion plots for the adsorption of Cd(II) onto POPDA/HZO

$$E = \frac{1}{\sqrt{2\,K_d}} \tag{15}$$

The values of mean free energy (E) were 5.0, 7.6, and 9.13 kJ mol^{-1} at 303, 313, and 323 K, respectively. Moreover, the R^2 values obtained for D-R isotherm model for adsorption of Cd(II) indicated a poor fit to the experimental data. Therefore, the mean energy calculated from D-R model could not necessarily explain the mechanism of adsorption.

On the basis of R^2 values, the order of best fit was Freundlich > Langmuir > Temkin > Dubinin-Radushkevich model at all temperatures. Moreover, error functions such as χ^2 and APE with respect to experimental adsorption capacity were also calculated. The error analysis indicated that Freundlich isotherm model described more accurately the adsorption of Cd(II) onto POPDA/HZO as compared to other isotherm models. This study also demonstrated that the adsorption occurred on heterogeneous surface with multilayer coverage.

Nonlinear fitting of isotherm models

Nonlinear isotherm models have also been applied to examine the equilibrium adsorption data. Microsoft Excel SOLVER function-spread sheet method was used to determine the isotherm parameters (Rahman and Nasir 2017; Hossain et al. 2013). Plots of q_e vs C_e using experimental and predicted values by nonlinear Freundlich model are shown in Fig. 9. The calculated coefficients for Langmuir (Fig. S9), Freundlich (Fig. 9), and Temkin (Fig. S10) isotherm models are summarized in Table 5. The values of R^2 obtained by linear regression method for Langmuir and Freundlich isotherm models were slightly higher than that obtained by nonlinear regression method at 303, 313, and 323 K. However, nonlinear regression method yielded higher R^2 values for Temkin model. Moreover, both linear and nonlinear fitting methods provided higher R^2 values and lowest values of error functions such as APE and χ^2 for Freundlich isotherm model at all temperatures studied. Therefore, it is concluded that

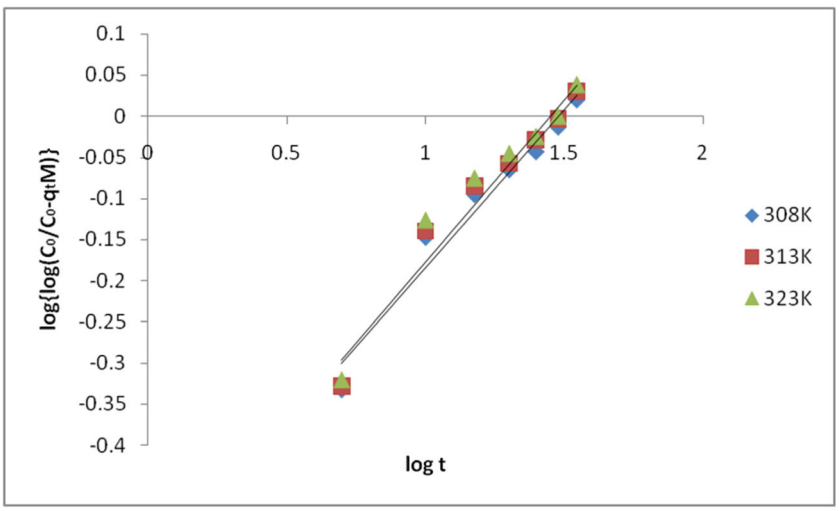

Fig. 13 Banghum's plots for the adsorption of Cd(II) onto POPDA/HZO

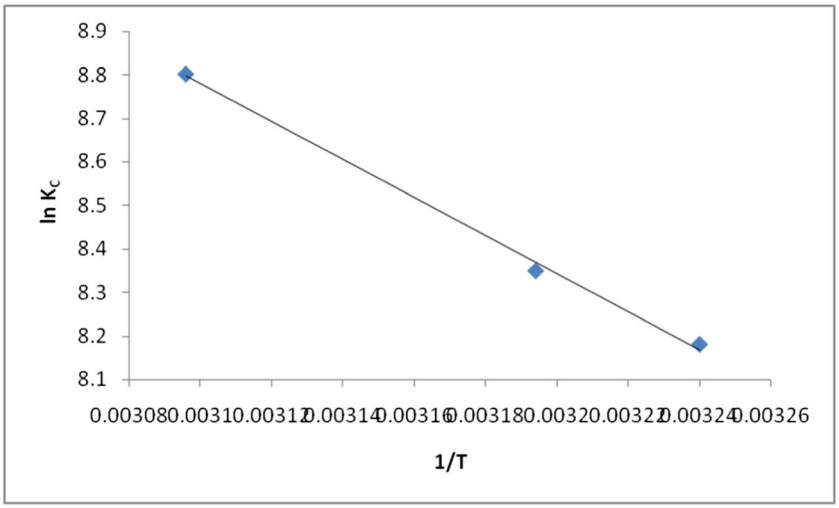

Fig. 14 Vant' Hoff plot for the adsorption of Cd(II) onto POPDA/HZO

Freundlich isotherm model successfully describes the adsorption of Cd(II) onto POPDA/HZO composite.

Adsorption kinetics

The kinetic adsorption data were examined by pseudo-first-order, pseudo-second order, intraparticle diffusion, Elovich, and Bangham's models to determine the rate of adsorption onto POPDA/HZO.

Pseudo-first-order kinetic model

The following equation represents the nonlinear form of pseudo-first-order kinetic model (Markandeya et al. 2015):

$$q_t = q_e\left(1-e^{-k_1 t}\right) \tag{16}$$

where k_1 is the pseudo-first-order rate constant (min^{-1}), q_e and q_t are the amount of Cd(II) adsorbed (mg g^{-1}) at equilibrium and at time t, respectively. The kinetic parameters were calculated by Microsoft Excel SOLVER function-spread sheet method (Hossain et al. 2013). Plots of q_t vs t for adsorption of Cd(II) at 303, 313, and 323 K are shown in Fig. S11. The values of k_1 and q_e (cal) were determined and summarized in Table 6.

Pseudo-second-order kinetic model

The rate of adsorption of adsorbate onto adsorbent can be described by pseudo-second-order kinetic model using the following nonlinear equation (Markandeya et al. 2015):

$$q_t = \frac{k_2 q_e^2 t}{1 + k_2 q_e t} \tag{17}$$

where k_2 is the rate constant (g mg^{-1} min^{-1}) for pseudo-second-order kinetics. The plots of q_t vs t at 303, 313, and 323 K are presented in Fig. 10. The values of k_2 and q_e were evaluated from Microsoft Excel SOLVER function-spread sheet method (Hossain et al. 2013) and summarized in Table 6. The best fitting of kinetic model for the adsorption of Cd(II) onto POPDA/HZO was judged on comparing the correlation coefficient (R^2) and calculated adsorption capacity. The values of correlation coefficient (R^2) for pseudo-second-order kinetic plots were > 0.99 at all temperatures studied while these values were < 0.97 for pseudo-first-order kinetic plots. Moreover, the adsorption capacity calculated from the plots of q_t vs t were very close to experimental adsorption capacity at all the temperatures studied for the pseudo-second-order kinetics. These results demonstrated that the kinetic data for adsorption of Cd(II) onto POPDA/HZO fitted well to the pseudo-second-order kinetic equation.

Elovich equation

Elovich model is mainly used to explain the chemisorption process and is expressed by the following equation (Wu et al. 2009):

$$q_t = \frac{1}{\beta} ln\ (\propto\beta) + \left(\frac{1}{\beta}\right) lnt \tag{18}$$

where α and β are initial rate of sorption (mg g^{-1} min^{-1}) and a constant(g mg^{-1}) that gives information about the extent of surface coverage, respectively. Figure 11 shows the plots of q_t vs ln t at three temperatures (303, 313, and 323 K) and values of α and β were evaluated from the linear plots and summarized in Table 6. As can be seen in the table that correlation coefficients (R^2) are greater than 0.97 at all the temperatures which indicated the good fit of Elovich equation to the experimental kinetic data. The applicability of Elovich model indicated that the adsorption of Cd(II) occurred through chemisorption process.

Table 7 Comparison of adsorption characteristics of cadmium(II) ions on various adsorbents

S. no.	Adsorbents	Contact time (min)	Optimum pH	Adsorption capacity (mg g^{-1})	Isotherm model	Ref.
1	Polyacrylamide-modified Fe_3O_4/MnO_2	400	6	39.05	–	Liu et al. (2018)
2	Ion-imprinted thiol-functionalized polymer	240	7	62.79	Langmuir	Kong et al. (2018)
3	Zeolite-based geopolymer	420	5.0	26.24	Langmuir	Javadian et al. (2015)
4	Polyaniline-grafted-chitosan	60	6.0	12.87	Langmuir	Karthik and Meenakshi (2015)
5	Granular-activated carbon-supported magnesium hydroxide	400	6	8.08	–	Wang et al. (2016)
6	Poly(vinyl alcohol) and amino-modified MCM-41	160	6	46.73	Langmuir	Soltani et al. (2018)
7	4-Amino-3-hydroxynaphthalene sulfonic acid-doped polypyrrole films	–	5	50.4	Langmuir	Sall et al. (2018)
8	Sugarcane bagasse	25	7	0.95	–	Moubarik and Grimi (2015)
9	Untreated coffee grounds	120	–	15.65	Langmuir	Azouaou and Mokaddem (2010)
10	Cork biomass	60	6	14.77	Langmuir	Krika et al. (2016)
11	Corn stalk xanthates	120	7	20.58	Langmuir	Zheng and Meng (2016)
12	Nanomaganetized biochar	120	5	16	–	Karunanayake et al. (2018)
13	*Portulaca oleracea* plant biomass	100	6	43.48	Langmuir and Freundlich	Dubey et al. (2014)
14	Sugarcane straw	30	4	7.78	Freundlich	Farasati et al. (2016)
15	Mesoporous treated sewage sludge	60	6	56.2	Langmuir	Ahsainea et al. (2017)
16	Iron oxide-coated sewage sludge	–	7	14.7	Langmuir	Phuengprasop et al. (2011)
17	Poly(o-phenylenediamine)/hydrous zirconium oxide	45	6	66.66	Freundlich	This work

Diffusion-based kinetics

Weber–Morris' intraparticle diffusion model was applied to investigate the influence of diffusion on sorption of Cd(II) onto POPDA/HZO. The rate of intraparticle diffusion can be evaluated from the following equation (Weber and Morris 1963):

$$q_{t=K_{id}} t^{\frac{1}{2}} + C_{id} \tag{19}$$

where k_{id} is the intraparticle diffusion rate constant (mg g^{-1} $min^{-1/2}$) and C_{id} is the intercept which provides information about the thickness of the boundary layer (mg g^{-1}). Figure 12 shows the plots of q_t vs $t^{1/2}$ for adsorption of Cd(II) onto POPDA/HZO at different temperatures (303, 313, and 323 K). The values of k_{id} and C_{id} were calculated for both the linear portions of the plot and summarized in Table 6. As can be seen in the Fig. 12, plots showed two distinct linear portions, indicating that two stages were involved in the sorption of Cd(II). In stage I (first linear portion), the rate of adsorption was high up to 10 min which was due to external surface adsorption through film diffusion from solution to adsorbent surface. In stage II, the rate of uptake is slow which can be attributed to intraparticle diffusion. From this study, it can be suggested that both external film and intraparticle pore diffusion mechanisms are involved in the sorption of Cd(II) onto POPDA/HZO composite.

Bangham's equation

Bangham's equation has been applied to gain insight into the pore diffusion, and it is expressed as follows (Inyinbor et al. 2016):

$$\log\left\{\log\left[\frac{C_e}{C_o} - q_t M\right]\right\} = \log\left(K_o \frac{M}{2.303\ V}\right) + \propto \log t \tag{20}$$

where M and V are adsorbent mass (g L^{-1}) and solution volume (mL), respectively. α and K_0 are the constants of Bangham's equation where the value of α is less than 1. Figure 13 shows the plots of $\log\left\{\log\left[\frac{C_e}{C_o} - q_t M\right]\right\}$ vs $\log t$ for the adsorption of Cd(II) onto POPDA/HZO at 303, 313, and 323 K. The parameters of Bangham's equation and

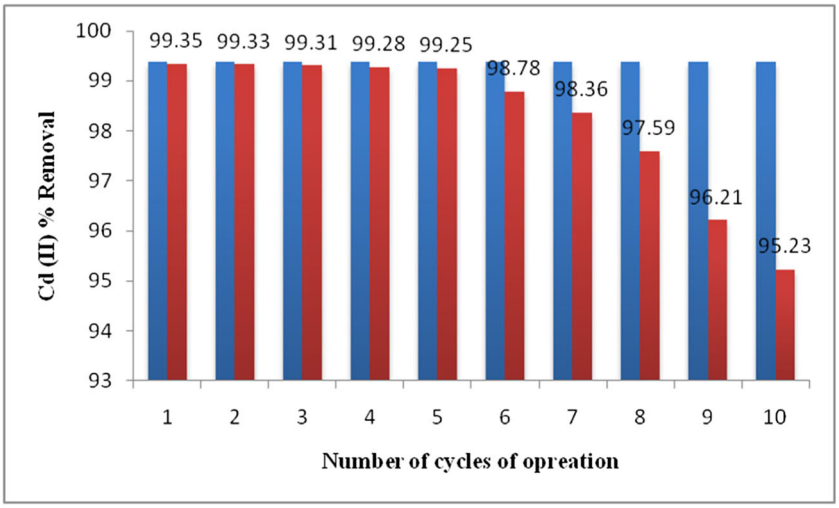

Fig. 15 Bar diagram shows the percentage uptake of cadmium by POPDA-Zr(IV)oxide in different cycles of batch operations

regression coefficients were evaluated from the linear plots (Fig. 13) and reported in Table 6. The values of R^2 were 0.961, 0.962, and 0.957 at 303, 313, and 323 K, respectively, which pointed that the kinetic data fitted well to Bangham's equation. Therefore, the sorption of Cd(II) onto POPDA/HZO can be regarded as pore diffusion-controlled process.

Thermodynamic studies

The effect of temperature on the adsorption of Cd(II) onto POPDA/HZO was studied which indicated that the extent of adsorption increased with increasing temperature. To gain an insight into the feasibility of adsorption, the values of ΔG^0, ΔH^0, and ΔS^0 were computed by considering the equations given below:

$$\Delta G^0 = -RT \ln k_c \tag{21}$$

$$lnk_C = \frac{\Delta S^0}{R} - \frac{\Delta H^0}{RT} \tag{22}$$

where k_c, R, and T are the equilibrium constant, universal gas constant (8.314 J K^{-1} mol^{-1}), and temperature (K), respectively. The values of equilibrium constant at different temperatures were calculated following the reported methods (Cadaval Jr. et al. 2016; Milonjic 2007). The values of ΔH^0 and ΔS^0 were evaluated from the linear plot of ln k_c vs $1/T$ (Fig. 14). The values of ΔG^0 were found to be − 20.606, − 20.726, and − 23.639 k J mol^{-1} at 303, 313, and 323 K, respectively, which pointed towards the spontaneous nature of the adsorption process and the spontaneity increases with increasing temperature. The value of ΔH^0 was 36.34 k J mol^{-1} which demonstrated the endothermic nature of the sorption process whereas the value of ΔS^0 (0.185 k J K^{-1} mol^{-1}) pointed towards the randomness on liquid/solid interface. All calculated thermodynamic data demonstrated that the uptake of Cd(II) onto POPDA/HZO is feasible and favorable process.

Comparison of adsorption characteristics of various adsorbents

The adsorption characteristics of various adsorbents for the removal of Cd(II) from water are shown in Table 7. The adsorption capacity of POPDA/HZO for Cd(II) ions was found to be 66.66 mg g^{-1}. Table 7 shows that the low cost adsorbents such as iron oxide-coated sewage sludge (Phuengprasop et al. 2011), sugarcane straw (Farasati et al. 2016), nanomagnatized biochar (Karunanayake et al. 2018), corn stalk xanthates (Zheng and Meng 2016), cork biomass (Krika et al. 2016), untreated coffee grounds (Azouaou and Mokaddem 2010), and sugarcane bagasse (Moubarik and Grimi 2015) possess Cd(II) adsorption capacity smaller than 21 mg g^{-1}. In addition, most of the low-cost adsorbents required longer time to achieve equilibrium. Mesoporous treated sewage sludge have showed a capacity of 56.2 mg g^{-1} and achieved equilibrium in 60 min. The results of adsorption of Cd(II) onto POPDA/HZO revealed that this material is superior to the low-cost adsorbents reported in the literature because it has higher adsorption capacity and requiring lesser time to achieve equilibrium. Other adsorbents such as polyacrylamide-modified Fe_3O_4/MnO_2 (Liu et al. 2018), ion-imprinted thiol-functionalized polymer (Kong et al. 2018), zeolite-based geopolymer (Javadian et al. 2015), granular-activated carbon (Wang et al. 2016), and poly(vinyl alcohol) and amino-modified MCM-41 (Soltani et al. 2018) required much longer time to achieve equilibrium. Moreover, the adsorption capacity of such materials for Cd(II) was lower than that of POPDA/HZO.

Desorption study

The desorption of Cd(II) from the adsorbent was studied by varying the concentration of NaOH (0.01–0.20 M). It was observed that the adsorbent was effectively regenerated (99.35%) by desorption of adsorbed Cd(II) by treatment of

Cd(II)-loaded POPDA/HZO with 0.20 M NaOH for about 20 min. The results demonstrated that the adsorption efficiency was maintained nearly constant up to six adsorption-desorption cycles, but after this, the efficiency decreased to a larger extent (Fig. 15). Therefore, it is concluded that POPDA/HZO composite material can be used effectively as an adsorbent for Cd(II) removal from polluted water.

Conclusion

A new adsorbent was prepared by incorporation of poly(o-phenylenediamine) into hydrous zirconium oxide for removal of Cd(II) from aqueous systems. The effects of experimental parameters on the removal percentage were investigated using BBD combined with RSM. The optimum variables to achieve 99.6% Cd(II) removal were determined by desirability function. The equilibrium data were fitted into various isotherm equations. On comparing the values of R^2, χ^2, and APS, it was judged that Freundlich isotherm model was the best model to describe the sorption of Cd(II). Elovich model suggested that chemisorption was involved in the uptake of Cd(II). The results of analysis of kinetic data indicated that the adsorption of Cd(II) onto POPDA/HZO obeyed the pseudo-second-order kinetic equation. The kinetic data were also analyzed by diffusion-based kinetics such as Weber-Morris intraparticle diffusion and Bangham's models. The results suggested the involvement of both external film and intraparticle pore diffusion mechanisms in the uptake of Cd(II). The desorption study revealed that POPDA/HZO can be used as potential sorbent to removal Cd(II) from polluted water.

Acknowledgements The authors are grateful to UGC (DRS-II) and DST (FIST and PURSE Phase II) for providing necessary research facilities. One of the authors (Mohd Nasir) is thankful to UGC for financial support.

Compliance with ethical standards

Conflict of interest The authors declare that they have no conflict of interest.

References

Ahamd AL, Shahbuddin MMH, Ooi BS, Kusumastuti A (2016) Cadmium removal from aqueous solution by emulsion liquid membrane (ELM): influence of emulsion formulation on cadmium removal and emulsion swelling. Desalin Water Treat 57:28274–28283

Ahsainea HA, Zbairb M, El Haoutia R (2017) Mesoporous treated sewage sludge as outstanding low-cost adsorbent for cadmium removal. Desalin Water Treat 85:330–338

Ali AAM, Zaki MI (1998) Fourier-transform laser Raman spectroscopy of adsorbed pyridine and nature of acid sites on calcined phosphate/Zr $(OH)_4$. Colloids Surf A Physicochem Eng Asp 139:81–89

Al-Malack MH, Al-Attas OG, Basaleh AA (2017) Competitive adsorption of Pb^{2+} and Cd^{2+} onto activated carbon produced from municipal organic solid waste. Desalin Water Treat 60:310–318

Anwar J, Shafique U, Zaman WU, Salman M, Dar A, Anwar S (2010) Removal of Pb (II) and Cd (II) from water by adsorption on peels of banana. Bioresour Technol 101:1752–1755

Azouaou N, Mokaddem H (2010) Adsorption of cadmium from aqueous solution onto untreated coffee grounds: equilibrium, kinetics and thermodynamics. J Hazard Mater 184:126–134

Badruddoza AZM, Shawon ZBZ, Daniel WJD, Hidajat K, Uddin MS (2013) Fe_3O_4/cyclodextrin polymer nanocomposites for selective heavy metals removal from industrial wastewater. Carbohydr Polym 91:322–332

Bandari F, Safa F, Shariati SH (2015) Application of response surface methodology for optimization of adsorptive removal of Eriochrome Black T using magnetic multi-wall carbon nanotube nanocomposite. Arab J Sci Eng 40:3363–3372

Bernard A (2008) Cadmium and its adverse effects on human health. Indian J Med Res 128:557–564

Boudrahem F, Soualah A, Aissani-Benissad F (2011) Pb (II) and Cd (II) removal from aqueous solution using activated carbon developed from coffee residue activated with phosphonic acid and zinc chloride. J Chem Eng Data 56:1946–1955

Cadaval TRS Jr, Dotto GL, Seus ER, Mirlean N, Pinto LAA (2016) Vanadium removal from aqueous solutions by adsorption onto chitosan. Desalin Water Treat 57:16583–16591

Candioti LV, Zan MMD, Camara MS, Goicoechea HC (2014) Experimental design and multiple response optimization using the desirability function in analytical methods development. Talanta 124:123–138

Cerrahoglu F, Kayan A, Bingol A (2017) New inorganic-organic hybrid materials and their oxides for removal of heavy metal ions: response surface methodology approach. J Inorg Organomet Polym 27:427–435

Chen G, Zeng G, Tang L, Du C, Jiang X, Huang G, Liu H, Shen G (2008) Cadmium removal from simulated wastewater to biomass byproduct of Lentinusedodes. Bioresour Technol 99:7034–7040

Derringer G, Suich R (1980) Simultaneous optimization of several response variables. J Qual Technol 12:214–219

Dey RK, Patnaik T, Singh VK, Swain SK, de Melo MA, Airoldi C (2010) Al-centered functionalized inorganic–organic hybrid sorbent containing N and S donor atoms for effective removal of cadmium. Solid State Sci 12:440–447

Ding Y, Jing D, Gong H, Zhou L, Yong X (2012) Biosorption of aquatic cadmium (II) by unmodified rice straw. Bioresour Technol 114:20–25

Directive 2006/11/EC of the European Parliament and of Council of 15 February 2006 on pollution caused by certain dangerous substances discharged into the aquatic environment of the community

Dou X, Mohan D, Pittman CU Jr, Yang S (2012) Remediating fluoride from water using hydrous zirconium oxide. Chem Eng J 198-199: 236–245

Dubey A, Mishra A, Singhal S (2014) Application of dried plant biomass as novel adsorbent for removal of cadmium from aqueous solution. Int J Environ Sci Technol 11:1043–1050

Farasati M, Haghighi S, Boroun S (2016) Cd removal from aqueous solution using agricultural wastes. Desalin Water Treat 57:1116–11172

Garg U, Kaur MP, Jawa GK, Sud D, Garg VK (2008) Removal of cadmium (II) from aqueous solutions by adsorption on agricultural wastes biomass. J Hazard Mater 154:1149–1157

Gavris G, Caraban A, Stanarel O, Badea GE (2013) Cadmium ions recovery by chemicals precipitation method from residual solutions of galvanic plating, J. Sustainable Energy 4:1–5

Gaya UI, Otene E, Abdullah AH (2015) Adsorption of aqueous Cd (II) and Pb (II) on activated carbon nanopores prepared by chemical

activation of doum palm shell. Springer Plus 4:458. https://doi.org/10.1186/s40064-015-1256-4

Georgescu I, Mureseanu M, Carja G, Hulea V (2013) Adsorptive removal of cadmium and copper from water by mesoporous silica functionalized with N-(aminothioxomethyl)-2-thiophen carboxamide. J Environ Eng 139:1285–1296

Gupta VK, Singh P, Rahman N (2005) Synthesis, characterization and analytical application of zirconium(IV) selenoiodate, a new cation exchanger. Anal Bioanal Chem 381:471–476

Hasanzadeh R, Moghadam PN, Bahri-Laleh N, Sillanpaa M (2017) Effective removal of toxic metal ions from aqueous solutions: 2-bifunctional magnetic nanocomposite base on novel reactive PGMA-MAn copolymer @ Fe_3O_4 nanocomposites. J Colloid Interface Sci 490:727–746

Heffron J, Marhefke M, Mayer BK (2016) Removal of trace metal concentration from potable water by electrocoagulation. Sci Rep 6: 28478. https://doi.org/10.1038/Sreo28478

Hegazi HA (2013) Removal of heavy metals from wastewater using agricultural and industrial wastes as adsorbents. HBRC J 9:276–282

Hema M, Srinivasan K (2011) Removal of cadmium (II) from wastewater using activated carbon prepared from agro industrial by products. J Environ Sci Eng 53:387–396

Hossain MA, Ngo HH, Guo W (2013) Introductory of Microsoft Excel SOLVER function-spreadsheet method for isotherm and kinetics modelling of metal biosorption in water and wastewater. J Water Sustainability 3:223–227

Huang M-R, Li X-G, Yang Y (2001) Oxidative polymerization of o-phenylenediamine and pyrimidylamine. Polym Degrad Stab 71: 31–38

Husein DZ, Aazam E, Battia M (2017) Adsorption of cadmium (II) onto watermelon rind under microwave radiation and application into surface water from Jeddah, Saudi Arabia. Arab J Sci Eng 42: 2403–2415

Ichinohe D, Saitoh N, Kise H (1998) Oxidative polymerization of phenylenediamines in reversed micelles. Macromol Chem Phys 199:1241–1245

Inyinbor AA, Adekola FA, Olatunji GA (2016) Kinetics, isotherms and thermodynamic modeling of liquid phase adsorption of rhodamine B dye onto Raphia hookerie fruit epicarp. Water Resour Ind 15:14–27

IS 10500 (1992) Drinking water specification (Reaffirmed 1993); http://www.hppcb.nic.in/ElAsorang/spec.pdf; 8.9.2007

Jain M, Garg VK, Kadirvelue K (2011) Investigation of Cr (VI) adsorption onto chemically treated Helianthus annuus: optimization using response surface methodology. Bioresour Technol 102:600–605

Javadian H, Ghorbani F, Tayebi H, Hosseini SM (2015) Study of the adsorption of cd (II) from aqueous solution using zeolite-based geopolymer, synthesized from coal fly ash; kinetic, isotherm and thermodynamic studies. Arab J Chem 8:837–849

Jimoh AA, Adebayo GB, Otum KO, Ajeboy AT, Bale AT, Jamiu W, Alao FO (2015) Sorption study of Cd (II) from aqueous solution using activated carbon prepared from Vitellaria paradoxa shell. J Bioremed Biodeg 6:288. https://doi.org/10.4172/2155-6199.1000288

Kakaei A, Kazemeini M (2016) Removal of Cd (II) in water sample using modified magnetic iron oxide nanoparticles. Iranian J Toxicol 10:9–14

Karthik R, Meenakshi S (2015) Removal of Pb(II) and Cd(II) ions from aqueous solution using polyaniline grafted chitosan. Chem Eng J 263:168–177

Karunanayake AJ, Todd OA, Crowley M, Ricchetti L, Pittman CU Jr, Anderson R, Mohan D (2018) Lead and cadmium remediation using magnetized and nonmagnetized biochar from Douglas fir. Chem Eng J 331:480–491

Kayan A, Arican MO, Boz Y, Ay U, Bozbas SK (2014) Novel tyrosine-containing inorganic-organic hybrid adsorbent in removal of heavy metal ions. J Environ Chem Eng 2:935–942

Kim E-J, Lee C-S, Chang Y-Y, Chang Y-S (2013) Hierarchically structured manganese oxide-coated maneticnano composites for the efficient removal of heavy metal ions from aqueous systems. ACS Appl Mater Interfaces 5:9628–9634

Kobya M, Demirbas E, Senturk E, Ince M (2005) Adsorption of heavy metal ions from aqueous solutions by activated carbon prepared from apricot stone. Bioresour Technol 96:1518–1521

Kong Q, Xie B, Preis S, Hu Y, Wu H, Wei C (2018) Adsorption of Cd^{2+} by ion –imprinted thiol-functionalized polymer in competition with heavy metal ions and organic acids. RSC Adv 8:8950–8960

Krika F, Azzouz N, Ncibi MC (2016) Adsorptive removal of cadmium from aqueous solution by cork biomass: equilibrium, dynamic and thermodynamic studies. Arab J Chem 9:51077–51083

Lin X, Burns RC, Lawrance GA (2005) Heavy metal ions wastewater: the effect of electrolyte composition on the precipitation of Cd (II) using lime and magnesia. Water Air Soil Pollut 165:131–152

Liu F, Jin Y, Liao H, Cai L, Tong M, Hou Y (2013) Facile self-assembly synthesis of titanate / Fe_3O_4 nanocomposites for the efficient removal of $Pb^{2+}$from aqueous systems. J Mater Chem A 1:805–813

Liu Z, Li X, Zhan P, Hu F and Ye X (2018) Removal of cadmium and copper from water by magnetic adsorbent of PFM: adsorption performance and microstructural morphology, Sep Purif Technol, (in press). https://doi.org/10.1016/j.seppur.2018.06.007

Mahmoud ME, Abdou AE, Ahmad SB (2016) Conversion of waste Styrofoam into engineered adsorbents for efficient removal of cadmium, lead and mercury from water. ACS Sustain Chem Eng 4: 819–827

Maleki A, Mahvi AH, Zazouli MA, Izanloo H, Barati AH (2011) Aqueous cadmium removal by adsorption on barley hull and barley hull ash. Asian J Chem 23:1373–1376

Markandeya, Shukla SP, Kisku GC (2015) Linear and nonlinear kinetic modelling for adsorption of disperse dye in batch process. Res J Environ Toxicol 9:320–331

Mehdinia A, Sehegfti S, Shemirani F (2015) Removal of lead (II), copper (II) and zinc (II) ions from aqueous solutions using magnetic amine-functionalized mesoporous silica nanocomposites. J Braz Chem Soc 26:2249–2257

Milonjic SK (2007) A consideration of the correct calculation of thermodynamic parameters of adsorption. J Serb Chem Soc 72:1363–1367

Mishra SP, Singh VK, Tiwari D (1996a) Efficient removal of zinc ions from aqueous solution by hydrous zirconium oxide. J Radioanal Nucl Chem 210:207–217

Mishra SP, Singh VK, Tiwari D (1996b) Radiotracer technique in adsorption study: part XIV. Efficient removal of mercury from aqueous solutions by hydrous zirconium oxide. Appl Radiat Isot 47:15–21

Mishra SP, Singh VK, Tiwari D (1997) Inorganic particulates in removal of heavy metal ions. Efficient removal of cadmium ions from aqueous solution by hydrous zirconium oxide. Radiochim Acta 76:97–101

Mohammed RR (2012) Removal of heavy metals from wastewater using black teawaste. Arab J Sci Eng 37:1505–1520

Mohanapriya T, Kumar PE (2016) Removal of cadmium (II) from aqueous solution on activated carbon prepared from Typha angustata L: equilibrium and kinetic studies. Int J Sci Res Publ 6:192–203

Mopoung R, Kengkhetkit N (2016) Lead and cadmium removal efficiency from aqueous solution by NaOH treated pineapple waste. Int J Appl Chem 12:23–35

Moubarik A, Grimi N (2015) Valorization of olive stone and sugar cane bagasse by-products as biosorbents for the removal of cadmium from aqueous solution. Food Res Int 73:169–175

Mourabet M, El-Rhilassi A, El-Boujaady H, Bennani-Ziatni M, El-Hamri R, Taitii A (2012) Removal of fluoride from aqueous solution by

adsorption on apatitic tricalcium phosphate using Box-Behnken design and desirability function. Appl Surf Sci 258:4402–4410

Muthirulan P, Kannan N, Meenakshsisundaram M (2013) Synthesis and corrosion protection properties of poly(o-phenylenediamine) nanofibers. J Adv Res 4:385–392

Nakamoto K (2009) Infrared and Raman spectra of inorganic and coordination compounds—part A: theory and applications in inorganic chemistry, 6th edn. John Wiley & Sons, Inc, Hoboken

Phuengprasop T, Sittiwong J, Unob F (2011) Removal of heavy metal ions by iron oxide coated sewage sludge. J Hazard Mater 186:502–507

Rahman N, Haseen U (2014) Equilibrium modeling, kinetic and thermodynamic studies on adsorption of Pb (II) by a hybrid inorganic-organic material :polyacrylamide zirconium (IV) iodate. Ind Eng Chem Res 53:8198–8207

Rahman N, Haseen U (2015) Development of polyacrylamide chromium oxide as a new sorbent for solid phase extraction of As (III) from food and environmental water samples. RSC Adv 5:7311–7323

Rahman N, Khan MF (2016) Nitrate removal using poly-o-toluidine zirconium (IV) ethylenediamine as adsorbent: batch and fixed-bed column adsorption modeling. J Water Process Eng 9:254–266

Rahman N, Nasir M (2017) Development of Zr(IV) – doped polypyrrole/zirconium(IV) iodate composite for efficient removal of fluoride from water environment. J Water Process Eng 19:172–184

Rahman N, Haseen U, Khan MF (2015) Cyclic tetra [(indolyl)-tetramethyl]-diethane-1,2-diamine (CTet) impregnated hydrous zirconium oxide as a novel hybrid material for enhanced removal of fluoride from water samples. RSC Adv 5:39062–39074

Rahmanidn B, Pakizeh M, Maskooki A (2012) Optimization of lead removal from aqueous solution by micellar-enhanced ultrafiltration process using Box-Behnken design. Korean J Chem Eng 29:804–811

Rao KS, Mohapatra M, Anand S, Venkateswarlu P (2010) Review on cadmium removal from aqueous solutions. Int J Eng Sci Technol 2:81–103

Rocha CG, Zaia DAM, Alfaya RVDS, Alfaya AADS (2009) Use of rice straw as biosorbent for removal of Cu(II), Zn(II), Cd(II) and Hg(II) ions in industrial effluents. J Hazard Mater 166:383–388

Rodriguez LA, Maschio LJ, da Silva RE, da Silva MLCP (2010) Adsorption of Cr(VI) from aqueous solution by hydrous zirconium oxide. J Hazard Mater 173:630–636

Sall ML, Diaw AKD, Sall DG, Biraud AC, Oturan N, Oturan MA, Fourdrin C, Huguenot D, Aason JJ (2018) Removal of lead and cadmium from aqueous solution by using 4-amino-3-hydroxynaphthalene sulfonic acid-doped polypyrrole films. Environ Sci Pollut Res 25:8581–8591

Salmani MH, Davoodi M, Ehrampoush MH, Ganeian MT, Fallahzadah MH (2013) Removal of cadmium (II) from simulated wastewater by ion floatation technique. Iranian J Environ Health Sci Eng 10:16. https://doi.org/10.1186/735-2746-10-16.

Samanta S, Roy P, Kar P (2017) Influence of structure of poly (o-phenylenediamine) on the doping ability and conducting property. Ionics 23:937–947

Seredych M, Bandosz TJ (2010) Effect of surface features on adsorption of SO_2 on graphite oxide/Zr $(OH)_4$ composites. J Phys Chem C 114:14552–14560

Singanan M (2011) Removal of lead (II) and cadmium (II) from wastewater using activated biocarbon. Sci Asia 37:115–119

Singh P, Rawat JP, Rahman N (2003) Synthesis and characterization of zirconium (IV) iodovanadate and its use as electron exchanger. Talanta 59:443–452

Singh R, Chadetrik R, Kumar R, Bishnoi K, Bhatia D, Kumar A, Bishnoi NR, Singh N (2010) Biosorption optimization of lead(II), cadmium(II) and copper(II) using response surface methodology and applicability in isotherm and thermodynamics modelling. J Hazard Mater 174:623–634

Socrates G (1980) Infrared Characteristic Group Frequencies. John Wiley & Sons, Ltd., Bristol, p 53:54,84

Soenarjo S, Wijaya C (2006) Adsorption behaviour of cadmium (II) on hydrous oxide inorganic resins. J Sains dan Teknologi Nuklir, Indonesia 7:131–145

Soltani R, Dinari M, Mohammadnezhad G (2018) Ultrasonic-assisted synthesis of novel nanocomposite of poly(vinyl alcohol) and amino-modified MCM-41: a green adsorbent for Cd(II) removal. Ultrason Sonochem 40:533–542

Tak B-Y, Tak B-S, Park Y-J, Yoon Y-H (2015) Optimization of color and COD removal from livestock wastewater by electrocogulation process: application of Box-Behnken design (BBD). J Ind Eng Chem 28:307–315

Talebi M, Abbasizadeh S, Ali R (2017) Evaluation of single and simultaneous thorium and uranium sorption from water systems by an electrospun PVA/SA/PEO/HZSM5 nanofiber. Process Saf Environ Prot 109:340–356

Tehrani MM, Abbasizadeh S, Alamdari A (2017) Prediction of simultaneous sorption of copper (II), cobalt (II) and zinc (II) contaminants from water system by a novel multi-functionalized zirconia nanofiber. Desalin Water Treat 62:340–417

US Environmental Protection Agency, International risk information system (IRIS) (1999) On cadmium. National centre for environmental assessment, Office of research and development, Washington, DC

Vekateswarlu S, Yoon M (2015) Rapid removal of cadmium ions using green-synthesized Fe_3O_4 nanoparticles capped with diethyl-4-(4amino-5-mercapto-4 H-1,2,4,-triazol-3-yl) phenyl phosphonate. RSC Adv 5:65444–65453

Venkatesan G, Senthilnthan U (2013) Adsorption batch studies on the removal of cadmium using wood of Derris Indica based activated carbon. Res J Chem Environ 17:19–24

Venkateswarlu S, Yoon M (2015) Rapid removal of cadmium ions using green-synthesized Fe_3O_4 nanoparticles capped with diethyl-4-(4amino-5-mercapto-4H-1,2,4-triazol-3yl) phenyl phosphonate. RSC Adv 5:65444–65453

Vilayatkar ND, Rahangdale PK, Donadkar DK (2016) Adsorption of cadmium (II) from solution onto activated carbon prepared from Madhucalongifolia fruit shell. Int J Adv Res 4:1360–1364

Wang C-W, Baroord JP, Mckay G (2014) Kinetic and equilibrium studies for the removal of cadmium ions by ion exchange resin. J Environ Chem Eng 2:698–707

Wang K, Zhao J, Li H, Zhang X, Shi H (2016) Removal of cadmium (II) from aqueous solution by granular activated carbon supported magnesium hydroxide. J Taiwan Inst Chem Eng 6:287–291

Weber WJ, Morris JC (1963) Kinetics of adsorption on carbon from solution. J Sanit Eng Div Am Soc Civ Eng 89:31–59

World Health Organization (2011) Cadmium in drinking-water, background document for development of WHO Guidelines for drinking-water quality

Wu F-C, Tseng R-L, Juang R-S (2009) Characteristics of Elovich equation used for the analysis of adsorption kinetics in dye-chitosan systems. Chem Eng J 150:366–373

Xu L, Zhuang Z (2014) Removal of cadmium ions from aqueous solution using chemically modified peanut shell. J Chem Pharm Res 6:646–653

Zhang JY, Wei Y, Li H, Zeng EY, You J (2017) Application of Box-Behnken design to optimize multi-solid phase extraction for trace neonicotinoids in water containing high level of matrix substances. Talanta 170:392–398

Zheng L, Meng P (2016) Preparation, characterization of corn stalk xanthates and its feasibility for Cd (II) removal from aqueous solution. J Taiwan Inst Chem Eng 58:391–400

Zong E, Wei D, Wan H, Zheng S, Xu Z, Zhu D (2013) Adsorption removal of phosphate ions from aqueous solution using zirconia-functionalized graphite oxide. Chem Eng J 221:193–203